Two-dimensional optics : diffraction and dispersion of surface plasmons
Chimento, P.F.

Author: Chimento, Philip
Title: Two-dimensional optics : diffraction and dispersion of surface plasmons
Issue Date: 2013-05-22

5
Surface plasmon coupling by attenuated total reflection for Drude-like metals

We discuss the influence of the optical properties of the metal used in a surface plasmon resonance experiment on the lineshape of the measured resonance curve. We also examine whether it is better to perform such experiments in the Kretschmann or Otto configuration, and find that the Otto configuration has some often-overlooked advantages. In addition, we present a phenomenological method for analyzing all possible lineshapes of surface plasmon resonance curves, that yields the complex surface plasmon mode index without a priori *knowledge of the composition of layers of metal and dielectric in the experiment.*

5.1 Introduction

This chapter has been submitted to *Optics Express* for publication.

A COMMON CONFIGURATION for studying surface plasmons at the interface between a metal and a dielectric is the attenuated total reflection setup. The most widely used variant is known as the Kretschmann configuration;[1] it is used in many applications, for instance in the bio-analytical sciences.[2] Various companies offer fully automated SPR analyzers for this purpose, starting with Biacore (now GE Healthcare) in the early 1990s;[3] Rich and Myszka[4] give an overview of recent devices.

An alternative to the Kretschmann configuration, known as the Otto configuration,[5] is much less frequently employed because it is generally presumed to be considerably more awkward experimentally. However, there are experimental systems where the Otto configuration outperforms the Kretschmann approach. One of the aims of the present chapter is to investigate when this applies and why that is so. We will also discuss the

[1] Kretschmann, 1971.

[2] Liedberg, Nylander, and Lunström, 1983.

SPR: surface plasmon resonance

[3] Rich and Myszka, 2008; Fivash, Towler, and Fisher, 1998.

[4] Rich and Myszka, 2010.

[5] Otto, 1968.

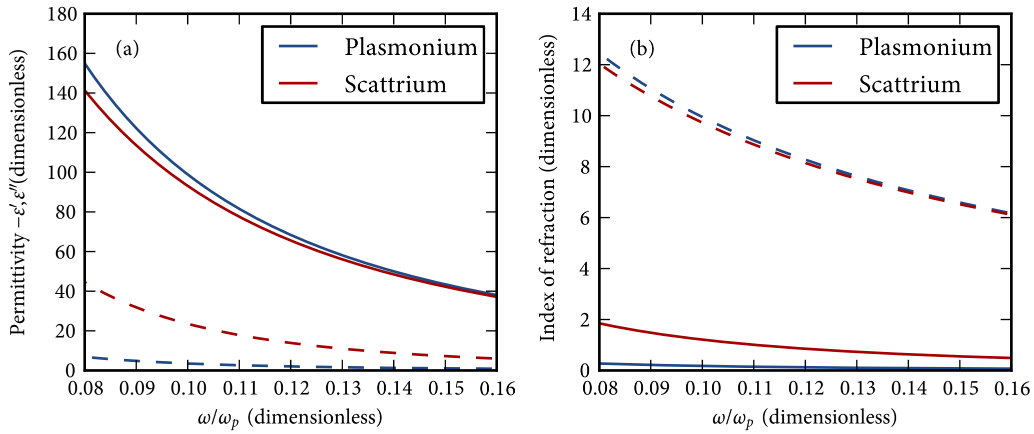

Figure 5.1: Dielectric function (a) and index of refraction (b) of the fictitious Drude metals plasmonium (blue) and scattrium (red). The solid lines, both left and right, indicate the real parts of the displayed quantity, and the dashed lines the imaginary parts. The real part of the dielectric function (solid line on left) is plotted with its sign flipped, i.e. as $-\varepsilon'$, so as to fit both quantities into a similar scale.

proper interpretation of SPR measurements when straying from the often-used metals of gold and silver.

We will base our discussion on the Drude model for the dielectric function of a metal:

$$\varepsilon(\omega) = 1 - \frac{\omega_p^2}{\omega(\omega + i\gamma)}, \tag{5.1}$$

where ω_p is the bulk plasma frequency of the metal and γ is the damping frequency related to the electron scattering time τ by $\gamma = 1/\tau$. The Drude model is a good approximation for many metals, in particular for the alkali metals such as lithium, sodium, and potassium. It applies also quite well to more mundane metals such as silver and aluminum for frequencies sufficiently far removed from an interband transition. We shall define dimensionless frequencies $\Omega = \omega/\omega_p$ and $\Gamma = \gamma/\omega_p$ so that the Drude model has only one material-dependent parameter:

$$\varepsilon(\Omega) = 1 - \frac{1}{\Omega(\Omega + i\Gamma)}.$$

In all interesting cases $\Gamma \ll 1$. The metallic regime is characterized by $\Omega < 1$.

FOR THE DISCUSSION AT HAND it is useful to introduce two fictitious Drude metals, which we will name plasmonium ($\Gamma = 0.0035$) and scattrium ($\Gamma = 0.025$). In this chapter, we will illustrate our findings with an octave of frequencies from $\Omega = 0.08$ to $\Omega = 0.16$, which is a relevant range for the analysis of our experiments on aluminum discussed in the next two chapters. Plasmonium is similar to an idealized version of silver, while for short wavelengths, scattrium is an idealized version of aluminum. The dielectric functions $\varepsilon = \varepsilon' + i\varepsilon''$ of plasmonium and scattrium are shown in Fig. 5.1. Note that for this choice of parameters, we can approximate $\varepsilon' \approx -\Omega^{-2}$ and $\varepsilon'' \approx \Gamma\Omega^{-3}$: the real parts of the dielectric functions ε' of the two Drude metals are nearly equal, but the imaginary parts ε'' differ by the ratio of the electron scattering times.

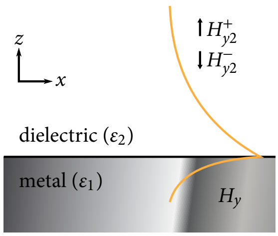

Figure 5.2: Sketch of an interface between two half-spaces of dielectric and metal. A typical H_y amplitude for the surface plasmon mode is sketched in orange. H_y must be continuous across the interface.

5.2 *Surface plasmons on an interface between two semi-infinite materials*

THE QUINTESSENTIAL SETTING for studying surface plasmons is the interface between a half-space ($z < 0$) of metal (with relative permittivity ε_1) and a half-space ($z > 0$) of dielectric (with relative permittivity ε_2). Figure 5.2 is an illustration of this situation. With the interface at $z = 0$, and assuming that the surface plasmons travel in the x direction, the surface plasmon field is fully determined by the y component of the magnetic field **H**. To determine this field we calculate the transfer matrix[6] for incoming and outgoing H_y amplitudes from both sides of the interface:

$$\begin{bmatrix} H^+_{y2} \\ H^-_{y2} \end{bmatrix} = \frac{1}{t_{21}} \begin{bmatrix} 1 & r_{21} \\ r_{21} & 1 \end{bmatrix} \begin{bmatrix} H^+_{y1} \\ H^-_{y1} \end{bmatrix}, \tag{5.2}$$

[6] Davis, 2009.

where $H^{\pm}_{yn}$ indicates the wave traveling in the $\pm z$ direction, and 1 and 2 represent the two half spaces. The coefficients r_{21} and t_{21} represent the interface reflection and transmission amplitudes, respectively.[7] These complex amplitudes are given by the well-known Fresnel relations (which imply that the appropriate fields are continuous across the interface):

[7] We note that $t_{12}t_{21} - r_{12}r_{21} = 1$ and $r_{12} = -r_{21}$.

$$r_{pq} = \frac{k_{zp}/\varepsilon_p - k_{zq}/\varepsilon_q}{k_{zp}/\varepsilon_p + k_{zq}/\varepsilon_q}, \qquad t_{pq} = \frac{2k_{zp}/\varepsilon_p}{k_{zp}/\varepsilon_p + k_{zq}/\varepsilon_q}. \tag{5.3}$$

Here $k_{zp}^2 = \varepsilon_p k_0^2 - k_x^2$, where $k_0 = \omega/c$ is the wave vector in vacuum. To find the plasmon mode we choose the sign of k_z in each half space such that the field H_y decays away from the interface. The allowed modes traveling along the interface in the x direction, i.e. the surface plasmons, follow from the requirement that they exist even if all incident fields (H^+_{y1}, H^-_{y2}) vanish. This requirement yields two surface plasmon modes traveling in the $\pm x$ directions, respectively:

$$\frac{1}{t_{21}} = 0 \implies \frac{k_{z1}}{\varepsilon_1} + \frac{k_{z2}}{\varepsilon_2} = 0 \implies k_x^\infty = \pm k_0 \sqrt{\frac{\varepsilon_1 \varepsilon_2}{\varepsilon_1 + \varepsilon_2}}. \tag{5.4}$$

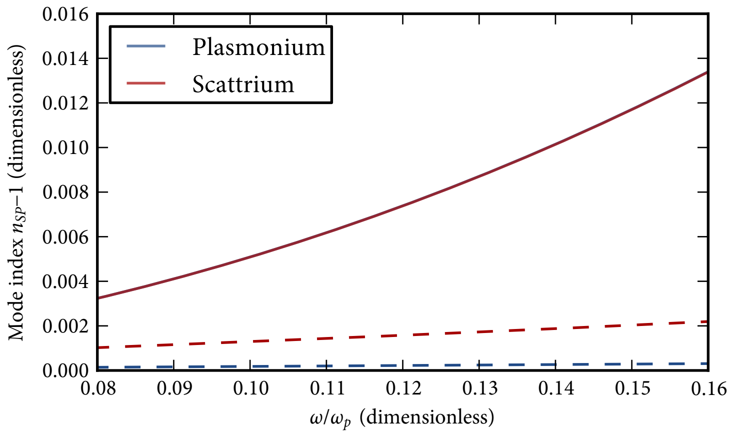

Figure 5.3: Effective mode index for a surface plasmon on an interface between vacuum and one of the fictitious metals plasmonium (blue) and scattrium (red). The solid lines (which coincide almost exactly) indicate the real part, and dashed lines the imaginary part. The real part of the index minus 1 is displayed so as to fit both quantities in a similar scale.

The result of (5.4) is the well-known surface plasmon dispersion relation on a flat interface between half-spaces; we use the notation k_{SP}^{∞} to emphasize that the materials are semi-infinite. Since ε_1 is complex-valued, the value for k_{SP}^{∞} that follows from (5.4) is also complex and can be written $k_{\mathrm{SP}}^{\infty} = k_{\mathrm{SP}}^{\infty\prime} + ik_{\mathrm{SP}}^{\infty\prime\prime}$: the surface plasmon propagates as a damped harmonic wave, with wavelength $2\pi/k_{\mathrm{SP}}^{\infty\prime}$ and $1/e$ amplitude damping length $1/k_{\mathrm{SP}}^{\infty\prime\prime}$.[8] It is convenient to introduce the complex surface plasmon mode index $n_{\mathrm{SP}}^{\infty} = k_{\mathrm{SP}}^{\infty}/k_0$. Figure 5.3 shows the dependence of the real and imaginary parts of this index for surface plasmons travelling along a metal–vacuum interface for plasmonium and scattrium, as a function of the frequency ratio Ω.

[8] This should not be confused with the intensity damping length $1/2k_{\mathrm{SP}}^{\infty\prime\prime}$, which some authors prefer.

When $|\varepsilon_1'|^2 > \varepsilon_1''^2$ and $\varepsilon_2 = 1$, we can approximate the mode index, by expanding the square root of a complex number, as

$$n_{\mathrm{SP}}^{\infty} \approx \sqrt{\frac{\varepsilon_1'}{\varepsilon_1'+1}}\left(1 + \frac{i\varepsilon_1''}{2\varepsilon_1'(\varepsilon_1'+1)}\right),$$

which shows that the real part of the mode index only depends on the real part of ε_1.[9] This explains why the real parts of the mode indices are almost exactly the same for plasmonium and scattrium.

[9] Raether, 1988, p. 5.

5.3 *Surface plasmons on a thin metal layer in the Kretschmann configuration*

INVESTIGATING SURFACE PLASMONS on a flat interface with semi-infinitely extending materials is confined to the realm of theory. In reality,

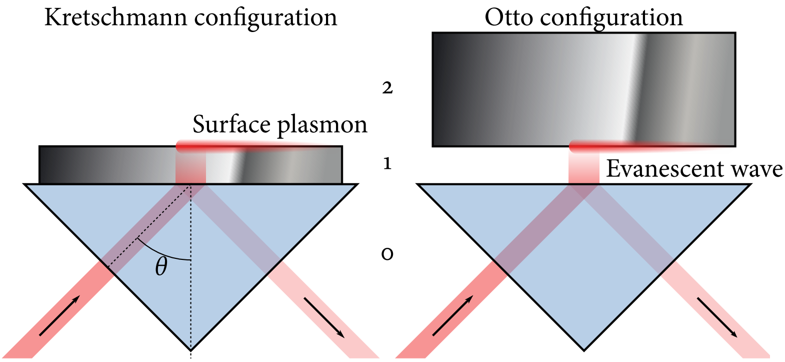

Figure 5.4: The Kretschmann and Otto variants of the attenuated total reflection method for exciting surface plasmons. In both cases, the evanescent wave from total internal reflection in the high-index dielectric (blue) phase-matches (in the direction parallel to the interface) to the surface plasmon mode on the interface between the metal (gray) and low-index dielectric (white).

one needs a way of coupling from freely propagating light to the confined surface plasmon mode and vice versa. Since the surface plasmon mode's wave vector (5.4) is larger than the free-space wave vector for a light wave of the same frequency, the difference in wave vector needs to be made up somehow. Popular methods of coupling to surface plasmons[10] include scattering from a corrugation on the metal surface,[11] increasing the wave vector by using one of the nonzero diffraction orders of a grating on the metal surface,[12] or having the light enter from a dielectric with an index of refraction n_0 that is higher than that of the dielectric that the surface plasmon travels on, so that the wave vector is increased by a factor of n_0.[13]

The latter method, which uses frustrated total internal reflection, has two variations, known as the Kretschmann and Otto configurations, illustrated in Fig. 5.4. Both involve a high-index dielectric substrate, medium 0, and a metal-dielectric interface 1–2. The metal is the thin layer 1 in the Kretschmann configuration, while the Otto configuration has a thin dielectric layer 1 and a bulk metal on top as medium 2. If the light is incident in medium 0 at an angle θ larger than the critical angle θ_{cr} for total internal reflection at the interface 0–1 (Otto) or 0–2 (Kretschmann), then the field[14] at the interface 0–1 can phase-match with the surface plasmon mode at the interface 1–2. When this happens, the reflection from the interface 0–1 takes a sharp dive, since the energy is instead transferred to the surface plasmon mode. This yields SPR curves such as that in Fig. 5.5. This is the principle behind SPR sensing. The angle at which the reflection is most attenuated is known as the resonance angle θ_{SPR}.

The depth of the reflectance dip is a measure for the coupling efficiency, and is a function of the metal layer's thickness. For each wavelength of the incident light, there is an optimum for the metal thickness at which the coupling is critical. At critical coupling, the internal damping is equal to the reradiation losses.[15]

[10] Sambles, Bradbery, and Yang, 1991.

[11] Jasperson and Schnatterly, 1969.

[12] Ritchie, Arakawa, Cowan, and Hamm, 1968.

[13] Kretschmann, 1971; Otto, 1968.

[14] In the Otto configuration, this field is evanescent.

[15] Raether, 1988, p. 12.

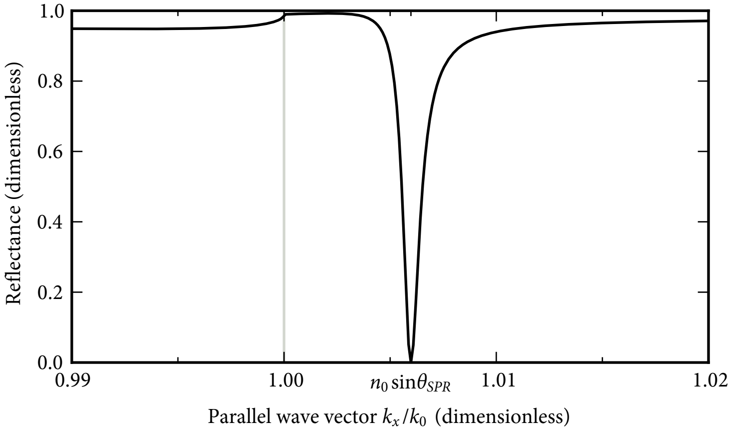

Figure 5.5: Typical SPR curve, here calculated for a plasmonium layer of critical coupling thickness on a glass-like substrate with $n = 1.5$, with vacuum on the outside. The critical angle for total internal reflection from substrate to vacuum is indicated by the gray line at $k_x = k_0$. The resonance angle θ_{SPR}, corresponding to a wave vector parallel to the interface $k_x = k_0 n_0 \sin\theta_{\mathrm{SPR}}$, is the angle at which the largest fraction of the incident light is absorbed into the surface plasmon mode.

In order to come to a set of equations for the surface plasmon in these multilayer stacks, we generalize (5.2) to N layers.[16] This is a powerful set of equations that contains everything we need to know about the system:

[16] Davis, 2009.

$$\begin{bmatrix} H_{yN}^{+} \\ H_{yN}^{-} \end{bmatrix} = \begin{bmatrix} M_{00} & M_{01} \\ M_{10} & M_{11} \end{bmatrix} \begin{bmatrix} H_{y0}^{+} \\ H_{y0}^{-} \end{bmatrix}, \tag{5.5}$$

where

$$\begin{bmatrix} M_{00} & M_{01} \\ M_{10} & M_{11} \end{bmatrix} = \left(\prod_{n=1}^{N-1} \frac{1}{t_{(n+1)n}} \begin{bmatrix} 1 & r_{(n+1)n} \\ r_{(n+1)n} & 1 \end{bmatrix} \begin{bmatrix} e^{ik_{zn}d_n} & 0 \\ 0 & e^{-ik_{zn}d_n} \end{bmatrix} \right) \times \frac{1}{t_{10}} \begin{bmatrix} 1 & r_{10} \\ r_{10} & 1 \end{bmatrix}. \tag{5.6}$$

As in the two-layer case, we can use this set of equations to calculate various properties of the system. The requirement of having a solution in the absence of incident fields yields

$$M_{11} = 0, \tag{5.7}$$

and solving this for complex k_x gives us the wave vector of the surface plasmon mode. The reflectance, on the other hand, is obtained by calculating the ratio of outgoing to incident power on the side of layer 0, with the condition of no incident field on the side of layer N,

$$R = \left| \frac{-M_{10}(k_x(\theta))}{M_{11}(k_x(\theta))} \right|^2, \tag{5.8}$$

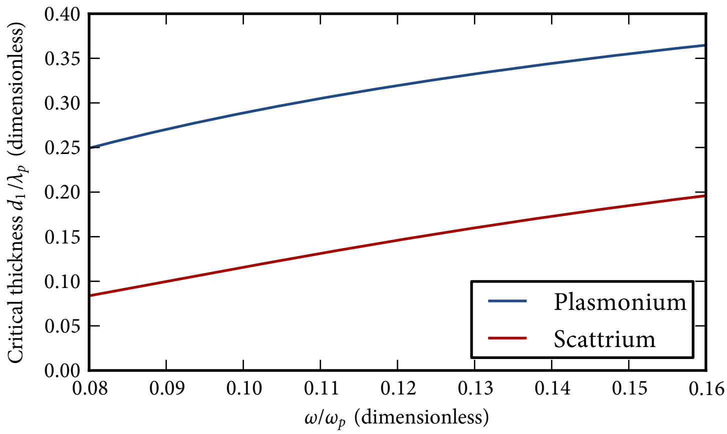

Figure 5.6: Free-space wavelength dependence of the metal thickness for critical coupling in a three-layer Kretschmann configuration of plasmonium or scattrium on a glass substrate with $n = 1.5$ and vacuum on the other side. Note that the critical thickness is given in units of the bulk plasmon wavelength $\lambda_p = \omega_p/2\pi c$.

with $k_x(\theta)$ the real-valued wave vector of the light incident from layer 0. On a related note, the thickness d_1 of layer 1 for which the reflectance vanishes is obtained by solving $M_{10} = 0$ for d_1 with the constraint that k_x is real.

The reflectance of a three-layer Kretschmann system can be written as:

$$R = \left| \frac{r_{01} + r_{12}\delta}{1 + r_{01}r_{12}\delta} \right|^2, \tag{5.9}$$

with $\delta = e^{2ik_{z1}d_1}$. The condition for surface plasmons (5.7) works out to $r_{01}r_{12}\delta = -1$.

Conversely, the condition for zero reflection and thus critical coupling, $M_{10} = 0$, is equivalent to setting the numerator to zero. It is instructive to write it thus:

$$-r_{01} = r_{12}\delta. \tag{5.10}$$

For unit field amplitude incident on the multilayer stack, r_{01} on the left-hand side of this equation gives the complex amplitude of the field as reflected from the glass-metal interface. The right-hand side represents the complex field amplitude at the glass-metal interface that has passed up and down through the metal film and has been reflected off the metal-air interface. Equation (5.10) means these two reflected waves with equal amplitudes interfere destructively in the direction of the reflected beam, yielding zero reflectance. All the power of the incident beam is coupled into the surface plasmon, which dissipates it away.[17] The critical coupling thickness for the two fictitious metals are shown in Fig. 5.6.

[17] Note that the critical coupling condition requires equality of two complex quantities.

Figure 5.6 shows that in the Kretschmann configuration, critical coupling is not easily lost when changing the wavelength of the incident light for a constant metal layer thickness. The difference in critical thickness between plasmonium and scattrium in Fig. 5.6 reflects the accelerated decay of the field in the lossier metal, and so a thinner layer is required to balance the two reflected fields.[18]

[18] As a reality check, we show that Fig. 5.6 does represent realistic numbers: for silver, a plasmonium-like metal with $\lambda_p = 138$ nm, (5.10) predicts a critical thickness of $0.34 \times 138 = 47$ nm for $\lambda = 1000$ nm ($\Omega = 0.138$). Likewise, for aluminum, a scattrium-like metal with $\lambda_p = 79$ nm, it predicts a critical thickness of $0.2 \times 79 = 14$ nm for $\lambda = 500$ nm ($\Omega = 0.16$).

[19] Raether, 1988, p. 12.

5.4 *Effect of electron scattering rate on the Kretschmann lineshape*

In traditional Kretschmann experiments where the dip in reflectance is very narrow because $|\varepsilon_1'| \gg 1$ and $\varepsilon_1'' \ll |\varepsilon_1'|$,[19] the dip is often approximated by a Lorentzian resonance subtracted from a constant background of unit magnitude. In this limit, the resonance angle gives the real part of the surface plasmon wave vector, and the half-width of the reflectance dip reveals the imaginary part. Repeating the measurement over a range of wavelengths yields the surface plasmon dispersion relation.

However, if $\varepsilon_1'' \ll |\varepsilon_1'|$ does not apply, then the reflectance yields much less information about the surface plasmon wave vector. Figure 5.7 illustrates this point by showing calculated Kretschmann reflectance curves at two different frequencies for a layer of plasmonium, which fulfills the conditions above, and a layer of scattrium, which does not fulfill $\varepsilon_1'' \ll |\varepsilon_1'|$. In the case of scattrium, even though the resonance angle and resonance width vary with the wavelength, it is difficult to say exactly how the resonance width should be defined, since the resonance is highly asymmetric. For example, the linewidths of the two curves in Fig. 5.7b are obviously different, but there is no apparent way to quantify them, since the lineshapes are asymmetric.

In fact, the rule of thumb that holds for plasmonium — that the resonance width yields information about the imaginary part of the surface plasmon wave vector — fails even on a basic intuitive level for scattrium: in Fig. 5.7, the purple curve's linewidth is, if anything, wider than that of the green curve, whereas one would expect it to be narrower because the resonance is more heavily damped at the higher frequency of the green curve, as we see from Fig. 5.3. The discrepancy is caused by the phase difference between the resonance and the background.

As we will show in the next section, the parallel wave vector at the resonance angle, $k_0\sqrt{\varepsilon_0}\sin\theta_{\mathrm{SPR}}$, does not necessarily correspond to the actual surface plasmon wave vector, contrary to what is usually assumed in Kretschmann experiments. In the case of a metal with low ε'' such as plasmonium, the difference is slight; but in scattrium, the actual surface

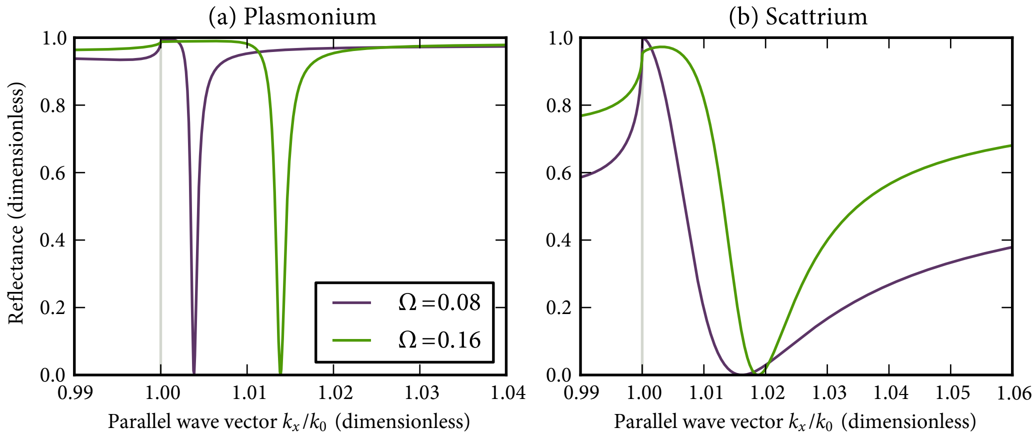

Figure 5.7: Calculated SPR curves for the Kretschmann configuration at two far-apart frequencies. The layers are plasmonium (a) and scattrium (b) on a $n = 1.5$ glass-like substrate. At each frequency, the layer is taken to have the proper thickness for critical coupling. The critical angle for total internal reflection in the substrate, at $k_x = k_0$, is indicated by a gray line. The curves in (a) are typical in SPR experiments. The position of the reflectance minimum corresponds to the real part of the wave vector of the surface plasmon, and its linewidth corresponds to the imaginary part. The scattrium-type curves in (b) are asymmetric without a well-defined linewidth. Their minimum does not correspond to the real part of the surface plasmon wave vector, and their width does not correspond to the imaginary part.

plasmon wave vector in scattrium is quite far removed from the parallel wave vector at the resonance angle. This finding is similar to a damped driven harmonic oscillator, where the damping parameter is related to ε''. It is well-known that a sufficiently damped, driven oscillator has its maximum response at a different frequency from the undamped resonance frequency. In fact, as we will see in the next section, a damped driven oscillator on a coherent background is precisely what describes the surface plasmon resonance.

5.5 *Analyzing Kretschmann lineshapes*

In his original paper, Kretschmann suggested considering the surface plasmon resonance a lightly damped driven oscillator, elegantly described by a Lorentzian lineshape.[20] The reflectance, in the neighborhood of the resonance angle, is then the resonance subtracted from a constant background of unit magnitude:[21]

$$R = 1 - \frac{4k_{\mathrm{SP}}^{\infty\prime\prime}\Delta k_{\mathrm{SP}}''}{(k_x - (k_{\mathrm{SP}}^{\infty\prime} + \Delta k_{\mathrm{SP}}'))^2 + (k_{\mathrm{SP}}^{\infty\prime\prime} + \Delta k_{\mathrm{SP}}'')^2}, \tag{5.11}$$

where k_{SP}^{∞} is the surface plasmon wave vector on the semi-infinite interface, as given by (5.4), and Δk_{SP} is a displacement that the resonance undergoes due to the presence of the coupling prism, approximated by:[22]

$$\Delta k_{\mathrm{SP}} = \frac{2|k_{\mathrm{SP}}^{\infty}|^3}{k_0^2(|\varepsilon_1'| + \varepsilon_2)} e^{2ik_{z1}d_1} r_{01}(k_{\mathrm{SP}}^{\infty}). \tag{5.12}$$

[20] Kretschmann, 1971.

[21] Raether, 1988, p. 12.

[22] Raether, 1988, p. 12.

However, as Fig. 5.7 clearly shows, this approximation does not fit very well to metals that behave like scattrium. In addition, it assumes that the resonance angle is equal to the angle corresponding to the surface plasmon wave vector. Various improvements to this fitting function exist, including ones that drop the latter assumption,[23] but there is little motivation to expand the analysis beyond plasmonium-type metals, since gold is most often used in commercial SPR systems anyway.

[23] Kurihara, Nakamura, and Suzuki, 2002.

HERE WE PRESENT A DESCRIPTION that is valid over a larger range of angles, not just in the neighborhood of the resonance, and can be used to fit metals with larger Drude scattering parameters. We start from the expression in (5.9) and write it as the coherent addition of a resonance to a slowly varying background. In addition, we note that r_{12}^{-1} goes to zero when $k_x = k_{\mathrm{SP}}^{\infty}$ (5.4) (the denominators of r_{12} and t_{12} are the same), so we write the expression as a function of r_{12}^{-1}:

$$r_{012} = \frac{r_{01} + r_{12}\delta}{1 + r_{01}r_{12}\delta} = r_{01} + \frac{(1 - r_{01})^2 r_{12}\delta}{1 + r_{01}r_{12}\delta} = r_{01} + \frac{(1 - r_{01})^2 \delta}{r_{12}^{-1} + r_{01}\delta} \tag{5.13}$$

Then we take a linear approximation of r_{12}^{-1} around the zero at k_{SP}^{∞}:

$$r_{12}^{-1} \approx \alpha(k_x - k_{\mathrm{SP}}^{\infty}), \qquad \alpha = \left.\frac{\partial}{\partial k_x} r_{12}^{-1}\right|_{k_x = k_{\mathrm{SP}}^{\infty}} \tag{5.14}$$

with α a complex-valued constant. So far, this is the same approach by which Kretschmann derived the Lorentzian resonance. However, instead of taking unit background and resonance amplitudes, we make no more approximations, instead writing the expression as follows:

$$R(k_x) = \left| B + \frac{A e^{i\phi} k''_{\mathrm{SP}}}{k'_{\mathrm{SP}} + i k''_{\mathrm{SP}} - k_x} \right|^2, k_x > k_{cr}. \tag{5.15}$$

We neglect the part of the reflectance curve under the critical angle, since the linear approximation breaks down at that point.

We can use this expression for extracting the surface plasmon wave vector from SPR curves. There are five fit parameters in the expression: B, the background amplitude; A, the resonance amplitude; ϕ, the phase difference between the background and resonance; and k'_{SP} and k''_{SP}, the complex surface plasmon wave vector. The advantage of this expression is that it yields a surface plasmon wave vector without requiring any advance knowledge of the composition or thicknesses of the layer system: it is completely phenomenological.

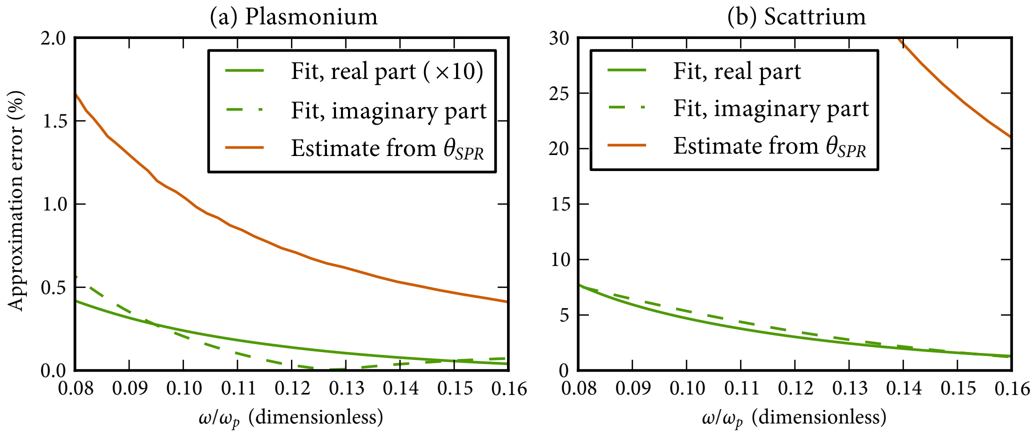

Figure 5.8: Plot of the relative error in the value of n_{SP} (green curves) made by using the value obtained from fitting the numerically calculated reflectance curves with (5.15). The orange curves are the result of simply estimating n'_{SP} from the resonance angle, which is a fairly good approximation for plasmonium (a), but not at all for scattrium (b). The error in the real part in (a) has been multiplied by 10 to improve visibility.

Figure 5.8 shows how effective the phenomenological fit is, compared to estimating the surface plasmon mode index from the resonance angle. On the vertical axis, we plot the approximation error, i.e. the deviation between the calculated and estimated mode index. For low-loss metals like plasmonium, the phenomenological fit proves excellent (error < 0.1%), but it is acceptable to use the resonance angle (error < 2%). For scattrium-like metals, the resonance angle is quite far off, whereas the phenomenological fit performs reasonably well.

As a comprehensive acid test for the phenomenological fitting procedure, we calculate SPR curves for a Kretschmann configuration experiment for a wavelength range from 500 to 800 nm. As a substrate we take BK7 glass with Sellmeier dispersion;[24] as metal we take a 40 nm layer of gold, the optical properties of which we approximate with a Drude model with added Lorentzian oscillators, fit to published values.[25] Gold is a plasmonium-like metal; however, around 500 nm, it has an interband absorption which increases the loss so that it enters a more scattrium-like regime. Therefore, this wavelength range nicely tests both symmetric and asymmetric SPR curves. We add an extra capping layer of 5 nm aluminum oxide with Sellmeier dispersion[26] to the calculations, in order to illustrate how the fitting procedure performs with more than three layers. Finally, we add Gaussian noise with a standard deviation of 1% to the signal. We then treat these data as measured results and fit them with (5.15). We show the results in Fig. 5.9.

In Fig. 5.9b, we see that the phenomenological fitting expression per-

[24] Schott AG, 2012.

[25] Rakić, Djurišić, Elazar, and Majewski, 1998.

[26] Babeva, Kitova, Mednikarov, and Konstantinov, 2002.

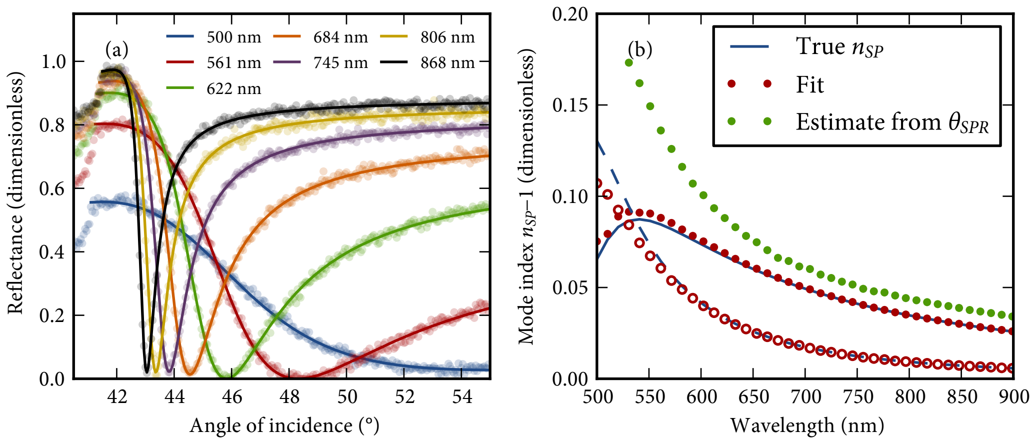

Figure 5.9: Performance of the phenomenological fitting expression of (5.15) on realistic, yet fictitious, SPR "measurements," calculated for a gold layer capped with Al_2O_3 on a BK7 substrate. (a) Generated fictitious data points for selected wavelengths, along with the corresponding fit as a solid line. Note the transition from a scattrium-like regime to a plasmonium-like regime as the wavelength increases. (b) Comparison of the calculated surface plasmon mode index n_{SP} (blue lines; real part solid, imaginary part dashed) to that obtained from the fitting procedure (red dots; real part closed, imaginary part open). For comparison, the green dots are the real part of the mode index estimated from the resonance angle.

forms admirably, much better in any case than estimating the real part of the mode index from the resonance angle. As the metal gets lossier and more scattrium-like, the fit gets slightly worse. It has a tendency to underestimate the imaginary part of the mode index, but that is not entirely surprising since the asymmetric dip is much wider than the "measured" angle range at 500 nm, as we see from the blue curve in Fig. 5.9a.

5.6 *Otto configuration*

THE OTTO CONFIGURATION (Fig. 5.4b) can be described by the same mathematics as the Kretschmann configuration. The only difference is that the thin layer ε_1 is a low-index dielectric and the metal ε_2 is on the outside. Because of this similarity, the Otto configuration is often considered equivalent to the Kretschmann configuration; but a common misconception is that there is practical difficulty in realizing it experimentally and it is therefore unattractive.

It is true that the original experimental realization of the Otto configuration, with air as the low-index dielectric, involves bringing the metal within a few microns of the prism and maintaining a constant air gap width over the entire surface, which was, and is even now, notoriously difficult to accomplish. For example, contamination by one or more dust particles of 75 μm[27] would make a one-micron air gap completely impossible. However, there is no reason why the low-index dielectric has to be air. For example, in chapters 6 and 7, we describe Otto experiments using

[27] ISO 4225:1994.

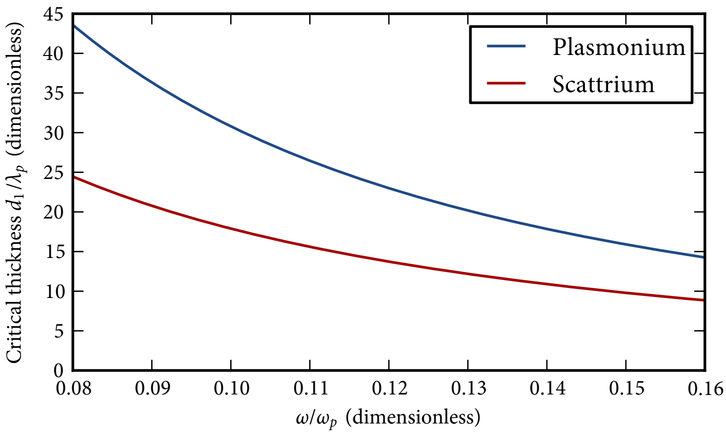

Figure 5.10: Free-space wavelength dependence of the gap thickness necessary for critical coupling in a three-layer Otto configuration of a glass substrate with $n = 1.5$ separated from bulk plasmonium or scattrium by a vacuum gap. Compare Fig. 5.6; the gap thickness is several orders of magnitude larger in the Otto configuration than the metal layer thickness in the Kretschmann configuration.

a high-index flint glass prism and magnesium fluoride as the low-index dielectric, where no gaps or moving parts are involved.

In this section, we will explore in which circumstances the Otto configuration is more appropriate for SPR measurements than the Kretschmann configuration. We will take the high-index dielectric to be a glass-like substance ($n = 1.5$) as before, the low-index dielectric to be vacuum, and the metal to be a bulk layer of either plasmonium or scattrium.

FIRST OF ALL, we use (5.10) to calculate the critical coupling thickness for the vacuum gap between the glass and the metal, shown in Fig. 5.10. In the Otto configuration, the middle layer must be several orders of magnitude thicker than the middle layer in the Kretschmann configuration in order to achieve critical coupling. This is because the surface plasmon's radiative losses must be equal to its damping losses at critical coupling, as we previously explained. A vacuum gap is lossless compared to a metal layer, and so the evanescent wave in the middle layer decays over a much larger distance in the vacuum gap than it does in the metal layer. If it has not decayed enough before bridging the gap, then the system is overcoupled. In addition, there is true total internal reflection at the glass-vacuum interface in the Otto configuration, whereas the wave in the metal layer in the Kretschmann configuration is not purely evanescent.

This is why the required layer thickness is many times that shown in Fig. 5.6; in order to balance the damping and reradiation losses, the field must cross a much larger distance compared to the Kretschmann case. Also, unlike the Kretschmann case, the critical coupling thickness now

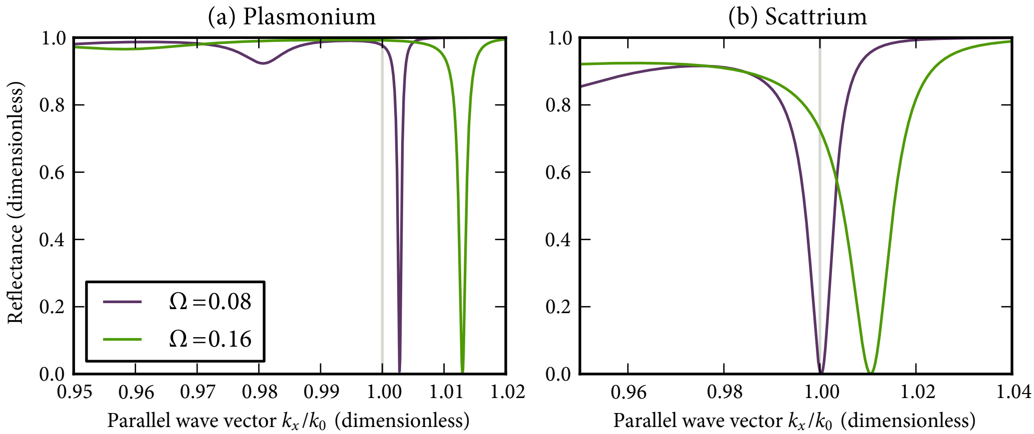

Figure 5.11: Calculated SPR curves for the Otto configuration at two far-apart frequencies. The outer layers are plasmonium (a) and scattrium (b), with a vacuum gap of critical coupling thickness (see Fig. 5.10 to read off the thickness) and an $n = 1.5$ glass-like substrate. The critical angle for total internal reflection in the substrate is indicated by a gray line. Compare Fig. 5.7.

exhibits a strong frequency dependence. The vacuum layer thickness d_1 scales approximately with i/k_{z1} (5.10); k_{z1}/k_0 is a small imaginary number, so $d_1 \propto 1/\omega$. This means that when designing an Otto experiment for a broad range of wavelengths, a middle layer of constant thickness will cause the resonance to become undercoupled or overcoupled much closer to the design wavelength than in the Kretschmann configuration.

We now examine the wavelength-dependent SPR curves for the Otto system. We show a number of examples in Fig. 5.11. There are some notable differences from the equivalent SPR curves for the Kretschmann system (Compare Fig. 5.7.)

For both plasmonium and scattrium, nothing special happens at the critical angle, unlike the Kretschmann case. This is because the Otto configuration deals with true frustrated total internal reflection, where the incident wave, which is evanescent in the gap, can still excite a propagating wave in the metal for some angles. The Kretschmann configuration, on the other hand, has the vacuum on the outside, so whether the light couples into the surface plasmon mode or not, it cannot travel into the vacuum in any case; the total internal reflection is not frustrated, only perturbed.

In addition, secondary resonances are visible at lower angles ($k_x < k_0$) than the main plasmonic resonances. Calculating the mode profile[28] shows that these are waveguide modes in the vacuum gap, as suggested by Tillin and Sambles.[29] The Kretschmann configuration's metal layer is

[28] Davis, 2009.

[29] Tillin and Sambles, 1988.

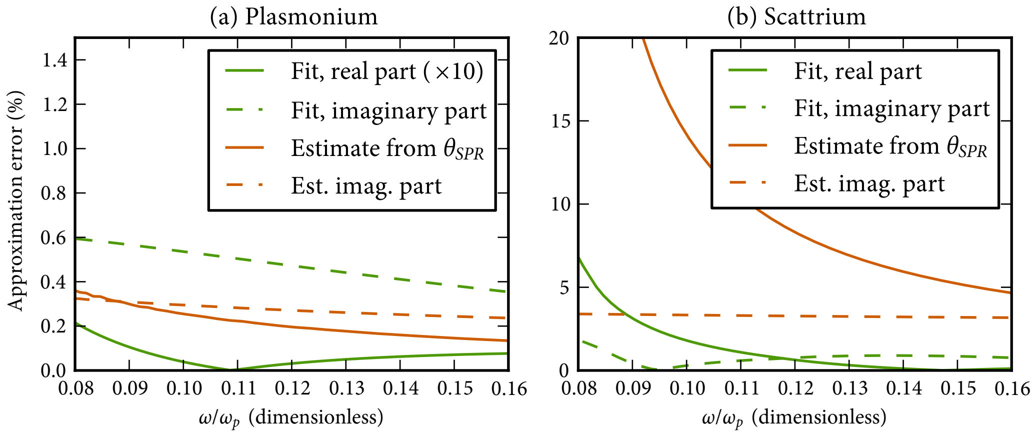

Figure 5.12: Plot of the relative error in the value of n_{SP} (green curves) made by using the value obtained from fitting the numerically calculated reflectance curves with (5.15). The orange curves are the result of simply estimating n'_{SP} from the resonance angle and n''_{SP} from the half-width, which is a good approximation for plasmonium (a), but not for scattrium (b). The error in the real part in (a) has been multiplied by 10 to improve visibility.

not thick enough to support such modes.

In both cases, the resonance lineshape is approximately Lorentzian and easy to interpret. Using the phenomenological fitting expression of (5.15), shown in Fig. 5.12, on the fictitious measurements of Fig. 5.11 shows that the analysis works well for both metals, performing comparably to the Kretschmann configuration. The resonance angle (making sure to take the resonance corresponding to the plasmon mode and not a waveguide mode) is a good indicator of the real part of the surface plasmon mode index for plasmonium, but not at all for scattrium. Again, this is because the approximation of (5.14) breaks down close to the critical angle.

Since the curves in Fig. 5.11 all have a reasonably well-defined linewidth, we can also estimate the imaginary part from the resonance's half-width at half-maximum. For scattrium, this yields reasonable results, but for plasmonium, this estimate is even slightly better than using (5.15). This indicates that, at least for the imaginary part of the mode index, the Otto configuration produces much more easily interpretable experimental results than the Kretschmann configuration when studying surface plasmons on a metal with large ε''.

5.7 *Conclusion*

WE HAVE DISCUSSED THE INFLUENCE of the optical properties of metals on the resonance lineshape in SPR measurements and examined the advantages and disadvantages of the Kretschmann and Otto configurations for SPR experiments.

We have demonstrated that there are advantages to the Otto configuration as a method of studying surface plasmons, contrary to what is often thought. In the case of a low-loss metal, such as our fictitious "plasmonium," it performs comparably to the Kretschmann configuration, although the Kretschmann configuration may be preferable if working with a large range of wavelengths. When working with high-loss metals such as our fictitious "scattrium," the resonance angle yields no information about the real part of the surface plasmon mode index in either configuration. However, the linewidth of an Otto curve is always a good indicator of the imaginary part of the mode index. Kretschmann curves, on the other hand, can be asymmetric for high-loss metals, in which case they do not have a well-defined linewidth.

In addition, the Otto configuration allows the use of arbitrarily thick layers of metal. This is important because a scattrium-type metal film must be very thin if used in the Kretschmann configuration: so thin, in fact, that the thickness is of the same order as the electron scattering length, possibly affecting the optical properties of the film.

We have also demonstrated a method for analyzing SPR curves that allows extraction of the complex surface plasmon mode index without any knowledge of the composition, thicknesses, or optical properties of the various layers of metal and dielectric involved in the attenuated total reflection coupling system. This phenomenological method of analysis yields values for the imaginary part of the mode index even when confronted with an asymmetric Kretschmann lineshape. It also yields more accurate values for the real part than can be obtained from the resonance angle, and works well for metals with large or small ε''.

Appendix 5.A Surface plasmon resonance curves beyond critical coupling

In this chapter, we have examined the critically coupled case of SPR, by adjusting the thickness of the middle layer (metal in the Kretschmann configuration, air in the Otto configuration) depending on the frequency of the incident light. This is not feasible in a real experiment, unless one is willing to deal with a layer of adjustable thickness, such as an oil layer whose thickness is changed by adjusting the mechanical pressure on the two surrounding solids;[30] even then, it is impossible to measure a broad range of wavelengths all at once.

[30] Quail, Rako, and Simon, 1983.

Therefore, in this appendix we evaluate a more realistic experimental situation for our fictitious metals plasmonium and scattrium. We take the plasma frequency of both metals to be $\hbar\omega_p = 15$ eV, allowing us to put in actual wavelengths; and we take a layer thickness appropriate to a wavelength of 800 nm ($\Omega = 0.10$). That is, in the Kretschmann configuration, 24.3 nm for plasmonium and 10.0 nm for scattrium; and in the Otto configuration, 2.4 μm for plasmonium and 1.4 μm for scattrium. We "measure" at six wavelengths, from 500 to 1000 nm.

Figure 5.13 shows the reflectance curves for the Kretschmann configuration. They are not so different from the curves in Fig. 5.7, bearing out our assertion that the coupling efficiency does not have a very strong dependency on the frequency in the Kretschmann configuration. It is interesting to note that the intuitive rule of thumb, that the resonance linewidth is related to the imaginary part of the surface plasmon wave vector, now seems to apply to scattrium; the blue ($\lambda = 500$ nm) resonance is broader in both plasmonium and scattrium, and this corresponds to more absorption in the metals at higher frequencies.

Figure 5.14, on the other hand, shows the reflectance curves for the Otto configuration. The secondary waveguide modes are once again visible at angles less than the critical angle, but this time they are closer to the critical angle. It is also immediately apparent that the coupling is much worse when the layer thickness is not optimized for critical coupling. The coupling to scattrium's surface plasmon mode at $k_x = 1.01k_0$ for $\lambda = 500$ nm is much weaker than the coupling to the waveguide mode at $k_x = 0.97k_0$. In plasmonium, the surface plasmon mode has all but disappeared at 500 nm, visible as a tiny blip at $k_x = 1.015k_0$.

Note that the main resonance in scattrium is not necessarily plasmonic at all wavelengths; it appears to the left of the critical angle, i.e. $k_{\mathrm{mode}} < k_0$, for $\lambda = 900$ and 1000 nm. It is a hybrid between a surface plasmon and

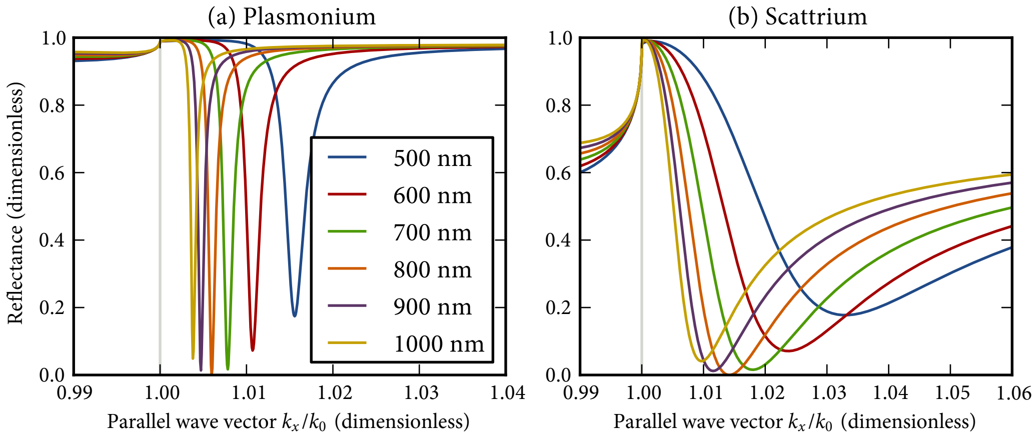

Figure 5.13: SPR curves for a number of representative wavelengths, for a Kretschmann experiment with (a) a 24.3 nm layer of plasmonium on a glass-like substrate with $n = 1.5$ surrounded by vacuum; (b) a 10.0 nm layer of scattrium on the same substrate, also in vacuum. The metal layers' thicknesses are designed for critical coupling at $\lambda = 800$ nm, but not for other wavelengths. Compare to Fig. 5.7.

waveguide mode, being strongly damped in the intermediate layer, but not entirely evanescent away from the interface. This emphasizes the modal character of the Otto plasmon; when the layer width is different from the critical layer width for surface plasmon mode, the effective index shifts.

In all cases, even for resonances away from critical coupling, the phenomenological expression of (5.15) still yields accurate results. The simpler method of extracting the real part of the surface plasmon wave vector from the resonance angle is a reasonable approximation in the Otto configuration, whereas it does not work in Kretschmann configuration if the lineshapes are asymmetric, as is the case with scattrium.

The conclusion stands, that the Otto configuration is a better experimental technique for probing surface plasmons on lossy scattrium-like metals. However, we note that if a broad enough wavelength range is required, then a constant gap width degrades the coupling to the surface plasmon mode, and in that case it is better to deal with the Kretschmann configuration's asymmetric lineshapes.

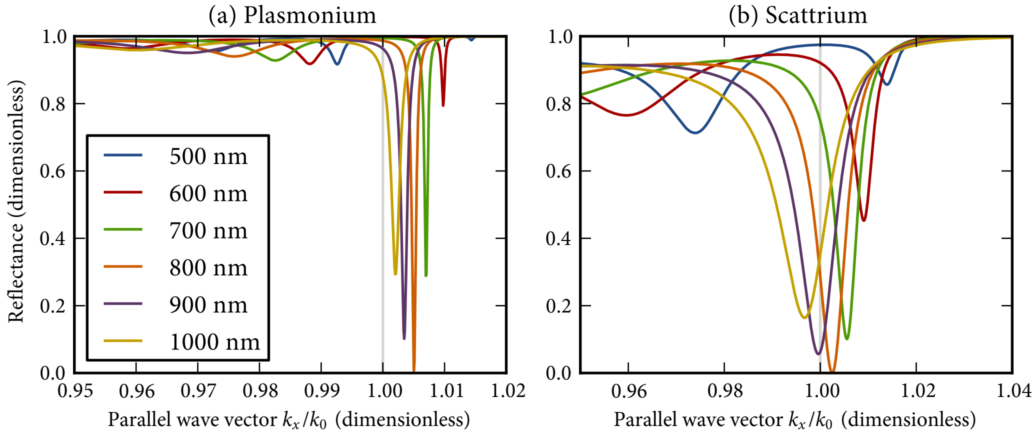

Figure 5.14: SPR curves for a number of representative wavelengths, for an Otto experiment with (a) plasmonium separated from a $n = 1.5$ glass-like substrate by a vacuum gap of 2.4 μm; (b) scattrium separated from the same substrate, by a vacuum gap of 1.4 μm. The gaps' thicknesses are designed for critical coupling at $\lambda = 800$ nm, but not for other wavelengths. Compare to Fig. 5.11.